Wind Energy

WIND ENERGY
Wind Energ. (2012)
Published online in Wiley Online Library (wileyonlinelibrary.com). DOI: 10.1002/we.1551

RESEARCH ARTICLE

Wind tunnel test on mean wind forces and peak pressures acting on wind turbine nacelles

Hiroshi Noda[1] and Takeshi Ishihara[2]

[1] Department of Architecture, Kinki University, 3-4-1 Kowakae, Higashiosaka, Osaka, Japan
[2] Department of Civil Engineering, The University of Tokyo, 7-3-1 Hongo, Bunkyo-ku, Tokyo, Japan

ABSTRACT

Mean wind force coefficients of nacelles are investigated by a wind tunnel test and are compared with those in current codes, such as the Germanischer Lloyd Guideline 2010 (GL2010) and Eurocode, in order to clarify the effects of the ground, presence of a hub, turbulence in the incident flow and nacelle length on these coefficients. Formulas for the mean wind force coefficients are proposed as a function of yaw angles. It is found that mean wind force coefficients of wind turbine nacelles specified in GL2010 are underestimated in comparison with those obtained by wind tunnel tests.

Pressure measurements of a nacelle are also conducted. Notably, the mean pressure coefficients for design load case 6.2 (DLC6.2) are significantly larger than those for design load case 6.1 (DLC6.1) in IEC61400-1. Maximum and minimum mean pressure coefficients are proposed for the DLC6.1 and DLC6.2 by the wind tunnel test, which are similar to those in Eurocode and are larger than those proposed in GL2010. Copyright © 2012 John Wiley & Sons, Ltd.

KEYWORDS
wind turbine nacelle; wind tunnel test; mean wind force; peak pressure

Correspondence
Hiroshi Noda, Department of Architecture, Kinki University, 3-4-1 Kowakae, Higashiosaka, Osaka, Japan.
E-mail: hnoda@arch.kindai.ac.jp

Received 11 June 2011; Revised 29 July 2012; Accepted 2 August 2012

1. INTRODUCTION

Mean wind force coefficients are necessary for the design of towers and foundations of wind turbines, and peak pressure coefficients of nacelles are required for designing the components and claddings of nacelles. Several studies[1–6] have been conducted on the mean wind force of towers and blades of wind turbines, but there is a paucity of those of nacelles. Nacelles have been severely damaged by extreme wind in Japan; underestimation of the peak pressure coefficients for the design of nacelle cladding was revealed by investigations of the accident.[7]

Germanischer Lloyd introduced mean pressure coefficients around the nacelle enclosure in its revised version of guideline GL2010.[8] Eurocode[9] also provided mean pressure coefficients. GL2010 is used for Design Load Case 6.1 (DLC6.1) in IEC61400-1,[10] and Eurocode[9] is used for the design of buildings. It is necessary to validate the applicability of those codes to the component and cladding designs of nacelles.

In this study, wind tunnel tests were conducted to investigate the mean wind force and peak pressure coefficients acting on wind turbine nacelles. The purpose of doing this was to determine the wind force coefficients and surface pressure coefficients that pertain to extreme wind load conditions. In this paper, first, the experimental setup of the wind tunnel tests, such as wind tunnel facilities, experimental winds, experimental models, and measurement methods, is described. The characteristics of wind force coefficients are then examined, and formulas for nacelle designs are proposed. Results of the pressure measurements and characteristics of the mean and peak pressure coefficients are then discussed. Finally, the distributions of the equivalent maximum and minimum mean pressure coefficients are proposed for design load cases of DLC6.1 and DLC6.2 in IEC61400-1.[10]

2. EXPERIMENTAL SETUP

The wind tunnel tests were designed to obtain the wind force and surface pressure coefficients of nacelles. The experimental setup, such as wind tunnel facilities, experimental winds, experimental models, and measurement methods, is presented in this section.

2.1. Experimental facilities and characteristics of indent flow

Experiments were conducted in an Eiffel-type wind tunnel with a test section size of 2.0 m (height) × 2.6 m (width) 37.6 m (length). The wind tunnel facility is shown in Figure 1. Smooth flow with a turbulence intensity of 0.2% and turbulent boundary layer flow were used as incident flows. Profiles of the mean wind speed and turbulence intensity of the incident flows are shown in Figures 2(a),(b). The power law exponent α was 0.2, and the turbulence intensity at the hub height was approximately 13% in the case of the turbulent boundary layer flow. Figure 2(c) shows the power spectrum density along the wind component in the case of the turbulent boundary layer flow. A von *Karman*-type spectrum is also plotted for comparison. It was found that the power spectrum density of the incident flow was very similar to the *Karman*-type spectrum. Characteristics of the incident flow, both smooth flow and turbulent boundary layer flow, were measured using a hot-wire anemometer.

Three parameters can be used to represent the incident flow in the case of the turbulent boundary layer: the power law exponent of the mean velocity, the turbulence intensity, and the turbulence scale. Representation of the turbulence scale is difficult and not significant; therefore, the turbulence scale was omitted in this paper. Incidentally, the turbulence scale of the turbulent boundary layer was 0.7 m and less than that recommended by IEC61400-1.[10]

2.2. Mean wind force measurements

The general configurations of the wind turbine nacelles are classified into four types: rectangular type, cylindrical type, globe type and disk type. The rectangular type is selected in this study because this type is commonly used for wind turbine nacelles. The aspect ratios of the nacelle models were determined by a survey of actual nacelle configurations, as shown in Figure 3. The scale of the model was chosen as 1/50; a schematic view of the model setup is shown in Figure 4. Nacelle models were connected to a load cell by a support rod that was shielded by a tower. The capacity range of the load cell was ±5 kg. The definitions of the wind forces and yaw angle are shown in Figure 5. The yaw angle is defined so that front surface is normal to the wind direction for $\theta = 0°$, and clockwise indicates positive yaw angles.

Wind force measurements were conducted for eight cases, as shown in Table I, in order to investigate the effects of the ground, presence of a hub, turbulence in the incident flow and nacelle length. A tower height of 400 mm was chosen, which is lower than the actual height of a wind turbine tower but is sufficient to avoid the effects of the ground on the wind force acting on the nacelle in the measurement. The blockage ratio of the nacelle was less than 1%. Therefore, the effects of blockage were not considered. Examples of the model setup are shown in Figure 6. Case 1 was designed to examine the effects of the ground and to compare the results with previous experimental results. Models in cases 1 and 2 did not have a hub, whereas those in other cases included a hub. Case 4 was for the top of a tower. The experimental conditions of the mean wind force measurements are summarized in Table II. Sampling time Δt was 10 ms (100 Hz), and the sampling number was 30,000. The yaw angle was changed

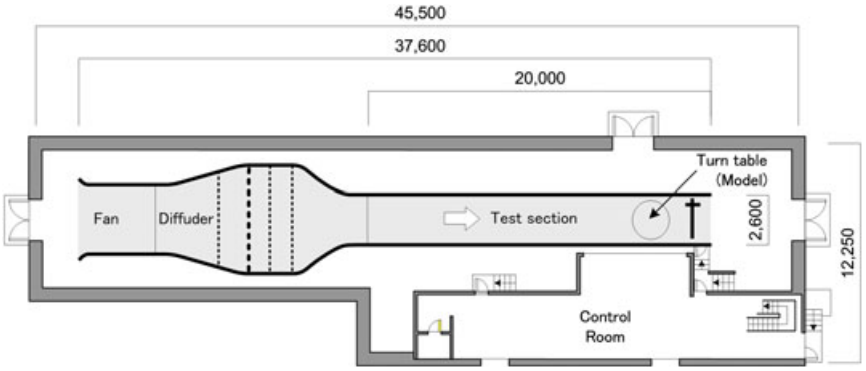

Figure 1. Wind tunnel facility.

DOI: 10.1002/we

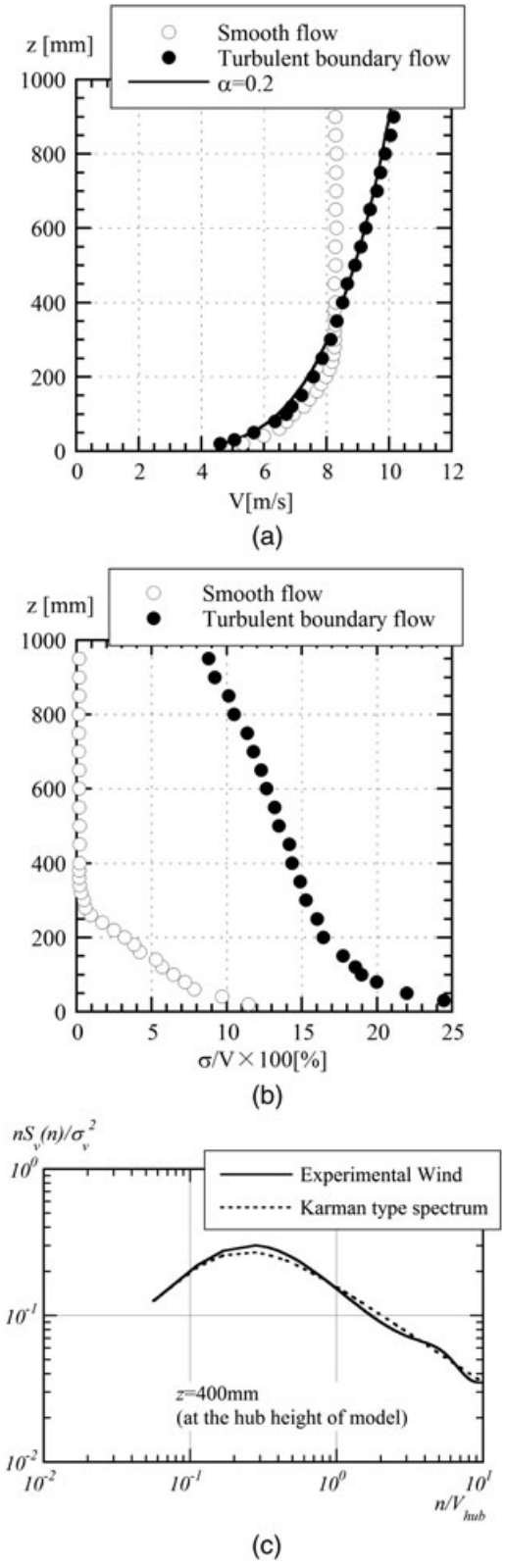

Figure 2. Characteristics of the incident flows: (a) vertical profiles of mean wind speed, (b) vertical profiles of turbulence intensity and (c) power spectrum of along wind component in turbulent boundary layer flow.

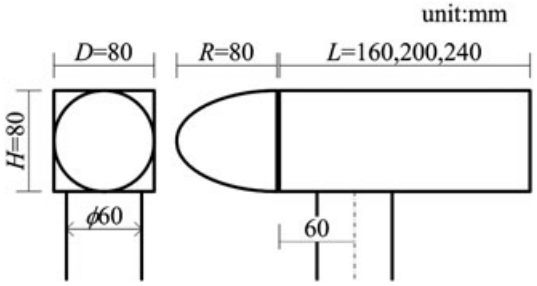

Figure 3. Experimental models.

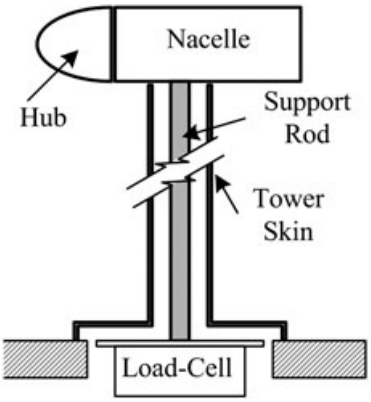

Figure 4. Setup of a model in wind force measurements.

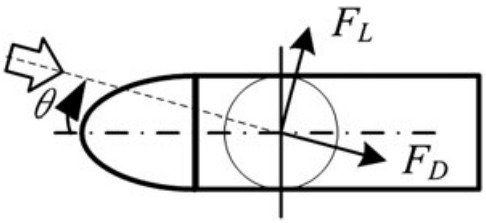

Figure 5. Definitions of forces and yaw angles.

Table I. Experimental cases for wind force measurements.

Case no.	Nacelle position	Hub	Intensity at nacelle height	Length ratio
Case 1	On the ground	Without	13%	L/D = 2.5
Case 2	On the top of tower	Without	13%	L/D = 2.5
Case 3	On the top of tower	With	13%	L/D = 2.0
Case 4	On the top of tower	With	13%	L/D = 2.5
Case 5	On the top of tower	With	13%	L/D = 3.0
Case 6	On the top of tower	With	0.2%	L/D = 2.0
Case 7	On the top of tower	With	0.2%	L/D = 2.5
Case 8	On the top of tower	With	0.2%	L/D = 3.0

from 0° to 180° at 5° intervals. The wind speed for the mean wind force measurement was $8\,\mathrm{m\,s^{-1}}$. The wind tunnel test for the sharp-edge model was independent of the Reynolds number in cases in which the Reynolds number was over 5000. The wind speed was, therefore, determined in relation to the sensitivity of the measuring instruments. The

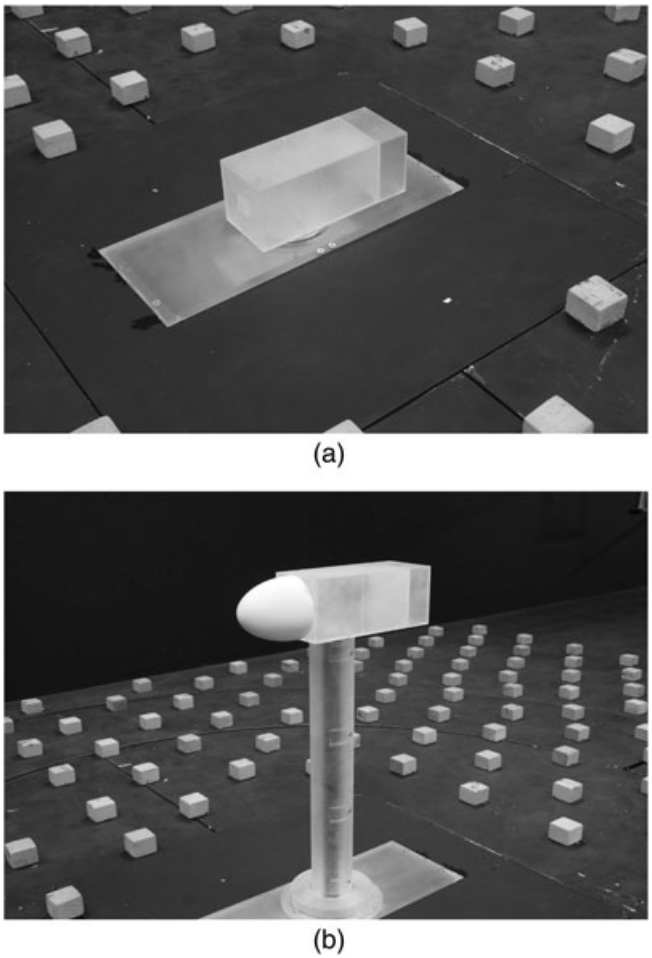

Figure 6. Examples of experimental setups for wind force measurements: (a) case 1 (on the ground) and (b) case 4 (on the top of tower).

Table II. Experimental conditions.

	Mean wind force measurements	Surface pressure measurements
Incident flows	Smooth flow/boundary layer flow	Boundary layer flow
Length scale	1/50	1/50
Wind speed at hub height	$8\,\mathrm{m\,s^{-1}}$	$13.5\,\mathrm{m\,s^{-1}}$
Reynolds number*	4.41×10^4	7.44×10^4
Sampling time (Δt)	10 ms	2.5 ms
Number of data	30,000	8192
Number of samples	1	10
Yaw angles	0°–180°	0°–180°

*Based on nacelle depth (=0.08 m).

Reynolds number based on the wind velocity at the hub height ($8\,\mathrm{m\,s^{-1}}$) and the nacelle depth (0.08 m) was 4.41×10^4 as determined by the mean wind force measurements.

2.3. Surface pressure measurements

The experimental model used for the surface pressure measurements was a model with a length-to-depth ratio of 2.5 and with a hub. The measurement was performed in the turbulent boundary layer flow, the same as in case 4 for the

wind forces measurements. All of the surface pressures were measured using pressure transducers connected to the surface pressure orifices by vinyl tubes. The range of each pressure transducer was ±248.9 Pa. The response time was 1 ms, and the low-pass filters were operated at 300 Hz. The amplifications and delays of fluctuating pressures due to the effect of the vinyl tubes were improved using the method proposed by Irwin *et al.*[11] In all, 187 pressure orifices were symmetrically arranged on one half-side of the model (Figure 7). Sampling time Δt was 2.5 ms (400 Hz), and the sampling number was 8192 per sample. The wind speed for the mean wind force measurements was 13.5 m s^{-1}. The Reynolds number based on the wind velocity at the hub height (13.5 m s^{-1}) and the nacelle depth (0.08 m) was 7.44×10^4 as determined by the surface pressure measurements. The experimental conditions of the surface pressure measurements are also summarized in Table II. The number of samples corresponds to the data set number. One data set is sufficiently stable for the mean wind force measurements. However, the peak pressures vary widely, and therefore, 10 data points were averaged to obtain maximum peak pressure coefficients.

To evaluate the peak values of the wind pressure that acts on a finite area, several pressure orifices should be arranged within this finite area and averaged in space. Instead of averaging the pressure in space, a moving average approach has been proposed by Lawson[12] and was applied to the time series of a sample of pressures using the equivalent averaging time T_c given as follows:

$$T_c = \frac{k \cdot l}{V_{\text{hub}}} \tag{1}$$

where l is the reference length of a finite area, V_{hub} is the wind velocity at the hub height and k is the decay constant. The decay constant k can be estimated by the root coherence of two pressure fluctuations as follows:

$$\sqrt{coh(n)} = \exp\left(-k\frac{n \cdot \Delta x}{V_{\text{hub}}}\right) \tag{2}$$

where n is the frequency (=1/T) and Δx is the separation distance between two pressures. A decay constant k of 4 was obtained from the wind tunnel test. The moving average number N required for T_c is given as follows:

$$N = \frac{T_c}{\Delta t} = \frac{k \cdot l}{\mathrm{V}_{\text{hub}} \cdot \Delta t} \tag{3}$$

where l is the assumed reference length, 1/50 m (The reference length is assumed as 1 m at full scale) and Δt is the sampling time. Therefore, the moving average number is estimated as 2.

This method is called as TVL method by which the size of the limiting eddy can be transformed into an average time or frequency by the mean velocity. This concept is similar to integrating the length of the wind velocity. A detailed description of the TVL method can be found in Lawson.[12]

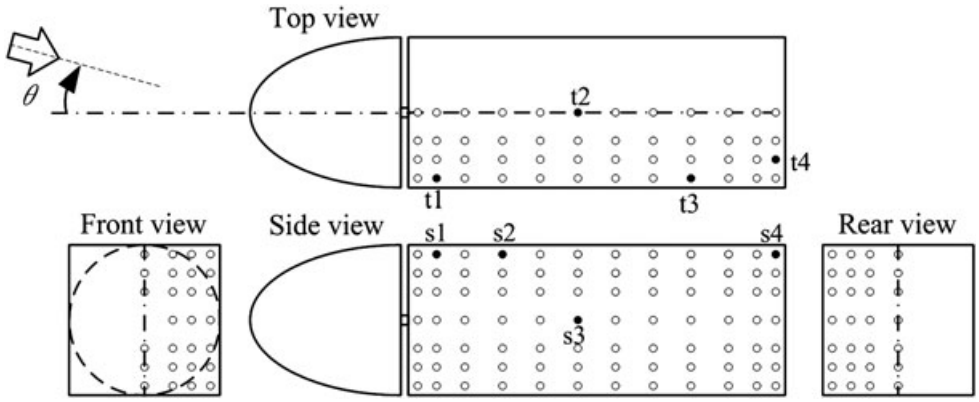

Figure 7. Pressure measurement orifices on a nacelle model.

The relationship between the full-scale time and the model-scale time is given as follows:

$$t_f = \frac{\gamma_\ell}{\gamma_V} t_m \tag{4}$$

where t_f and t_m are the full-scale time and model-scale time, respectively, γ_ℓ is the length ratio between the full scale and the model scale $\left(= \ell_f/\ell = 50\right)$ and γ_V is the velocity ratio.

According to IEC61400-1,[10] the period for evaluation of the peak pressure coefficients should be 10 min. For surface pressure measurements, the required sampling period in the model scale is 40 s, which is calculated using equation (4). This means that two samples should be used to evaluate the peak pressure coefficients because the sampling period of a surface pressure measurement is 20.5 s. Subsequently, five maximum and minimum peak values at the same yaw angles were averaged and used to define the maximum and minimum peak values for an evaluation time of 600 s in the full scale.

3. MEAN WIND FORCE COEFFICIENTS

The mean wind force coefficients are important parameters in the design of wind turbines that can sustain extreme winds. This section discusses the characteristics of the mean drag and lift coefficients obtained by the mean wind force measurements. The effects of various factors, such as those of the ground, presence of a hub, turbulence in the incident flow and nacelle length, on the coefficients are examined. Formulas for the mean drag and lift coefficients are proposed and compared with the current codes.

3.1. Definitions of mean wind force coefficients

The mean drag ($C_{\mathrm{D}}(\theta)$) and lift ($C_{\mathrm{L}}(\theta)$) force coefficients are defined as in equations (5) and (6), respectively:

$$C_{\mathrm{D}}(\theta) = \frac{F_D(\theta)}{\frac{1}{2}\rho {V_{\mathrm{hub}}}^2 A} \tag{5}$$

and

$$C_{\mathrm{L}}(\theta) = \frac{F_L(\theta)}{\frac{1}{2}\rho {V_{\mathrm{hub}}}^2 A} \tag{6}$$

where $F_{\mathrm{D}}(\theta)$ is the mean drag force, $F_{\mathrm{L}}(\theta)$ is the mean lift force, ρ is the air density, θ is the yaw angle, V_{hub} is the wind velocity at the hub and A is a reference area defined as in equation (7).

$$A = \pi DH/4 + LH \tag{7}$$

Here, $\pi DH/4$ indicates that the area of the hub is zero for cases 1 and 2, which do not include a hub. V_{hub} in equations (5) and (6) needs to be changed to V_{H}, which is the wind speed at the model height from the ground in case 1 (i.e. $H = 80$ mm). $F_{\mathrm{D}}(\theta)$ and $F_{\mathrm{D}}(\theta)$ were measured by a load cell installed at the bottom of the model as shown in Figure 4.

Figure 8 shows C_{D} and C_{L} versus the yaw angle in case 1, in which the rectangular model was set on the ground. The overall C_{D} and C_{L} distributions are in good agreement with the results of previous studies.[13,14]

3.2. Effects of various factors on mean wind force coefficients

First, the effects of the ground and hub on the drag and lift force coefficients are shown in Figure 9. The drag and lift force coefficients in all cases in Figure 9 are defined by the reference area LH instead of equation (7), for comparison. From comparison with case 1 on the ground and case 2 on the top of the tower, the increase in C_{D} by the ground effect is almost 20% at around $\theta = 90°$. The ground effects on C_{D}, therefore, are obvious in this study. Owing to the absence of ground effects, the wake that was recirculating the flow immediately behind the nacelle formed clearly, and the base pressures increased. The values of the drag force coefficients in case 2, therefore, were larger than those in case 1. This phenomenon

is conspicuous around 90°, when the depth-width ratio of the nacelle is small. In the case of around 0° and 180°, when the depth-width ratio is large, the separation flow is reattached on the side surface, and the wake is not clear. Therefore, an increase in the value of C_D is not seen.

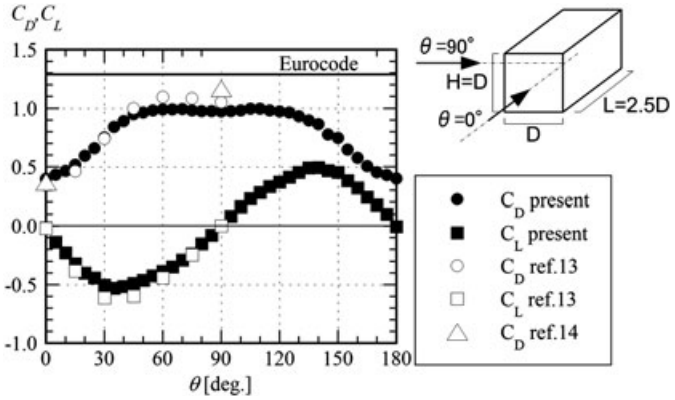

Figure 8. Comparison of previous studies for rectangular.

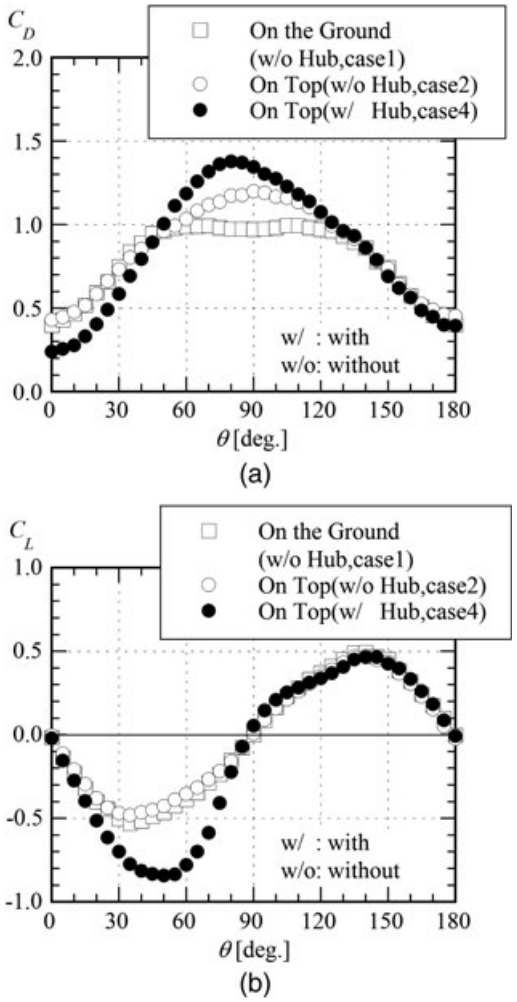

Figure 9. Effects of hub and ground on (a) C_D and (b) C_L defined by *LH* as reference area.

The maximum values of C_D for case 2 (without a hub) and case 4 (with a hub) are found near $\theta = 90°$ and are 1.2 and 1.4, respectively. The values of the drag coefficients in case 4 (with the hub) in the range of 50° to 100° are larger than those in case 2 (without a hub) because the projected area increases by the addition of the hub. The maximum increase in C_D caused by the hub is almost 23% at $\theta = 75°$, whereas decreases in C_D by the effects of the hub are observed in the yaw angle range of 0° to 45°. The reason for the deceases in C_D seems to be the decrease in the separation flow when the hub was located on the upwind side. The minimum values of C_L are found near $\theta = 45°$ and are -0.5 and -0.8 for cases without and with the hub, respectively.

The effects of inflow turbulence are shown in Figure 10. Notably, C_D and C_L are not affected by turbulence. A slight reduction in C_D in turbulent flow may be identical to that for a bluff body, such as a rectangular cylinder, whereas the wake decreases and the base pressure recover from turbulence in the incident flow.[15] The separation point of the flow was on the hub at around $\theta = 65°$. The hub has a curved shape, and consequently, the separation point was unstable. The instability of the separation point in the smooth flow is more conspicuous than that in the turbulent flow. The discontinuity of C_L, therefore, appears at around $\theta = 65°$ in the smooth flow (case 7).

Finally, the variations of C_D and C_L with nacelle lengths were investigated and are shown in Figure 11. Changes in C_D with changing length-to-depth ratios could be found at around 0° and 180°. These angles are almost normal to the models. This is similar to the results obtained by Nakaguchi *et al.*[16] for the mean drag coefficients of two-dimensional rectangular cylinders with different length-to-depth ratios. Values of C_L show a slight change with varying length-to-depth ratios. Because equation (7) is adopted as a reference area, changes in C_D and C_L with changing length-to-depth ratios are negligible. The discontinuity of C_L appears at around $\theta = 65°$ and $\theta = 145°$ in Figure 11(b). This discontinuity is caused by the instability of the separation point of flow on the curved hub, which is identical to the shape shown in Figure 10(b).

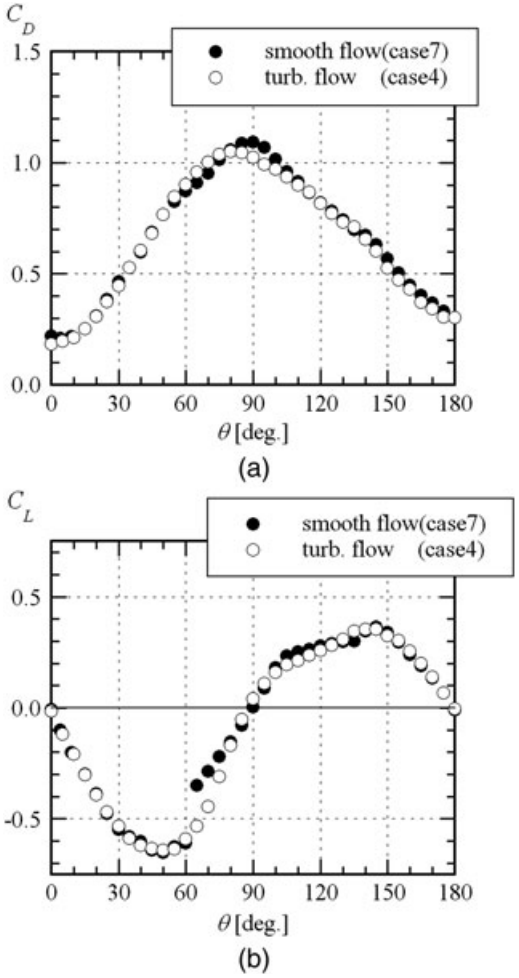

Figure 10. Effects of turbulence in incident flow on (a) C_D and (b) C_L.

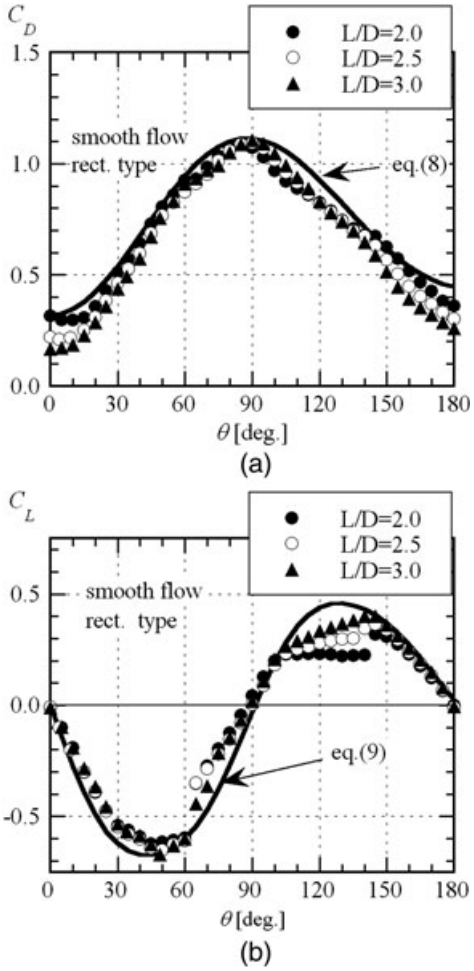

Figure 11. Effects of nacelle lengths on (a) C_D and (b) C_L in a smooth flow.

3.3. Formulas for mean wind force coefficients

Formulas for the mean drag and lift force coefficients of nacelles can be estimated as a function of yaw angles because the characteristics of C_D and C_L are nearly independent of the length-to-depth ratios. The wind force coefficients for an extreme wind load that acts on the nacelles are expressed as in equations (8) and (9).

$$C_D(\theta) = -0.36\cos(1.9\theta) - 0.06\cos(2.8\theta) + 0.74 \tag{8}$$

$$C_L(\theta) = \{-0.7\sin(2\theta) + 0.06\sin(2.3\theta)\}\cdot\{1.2 + 0.1\cos(4\theta)\}\cdot\cos(0.38\theta) \tag{9}$$

Wind force coefficients predicted by the proposed formulas in the yaw angle range of $\theta = 0^\circ$ to $\theta = 180^\circ$ are compared with experimental results as shown in Figure 11. Equations (8) and (9) are in good agreement with the experimental results. For simplicity, these proposed formulas are represented with trigonometric functions. Therefore, some deviations from the experimental results are observed. The proposed formulas provide slightly conservative results.

To compare our results for the coefficients with those in GL2010[8] and Eurocode,[9] the reference area is defined by the project area as a function of the yaw angle.

$$A(\theta) = |HR\cos\theta| + |LH\sin\theta| \tag{10}$$

Figure 12 shows that the maximum value of C_D obtained by the wind tunnel test is 1.4, whereas C_D in GL2010[8] and Eurocode[9] is slightly underestimated at 1.3. It seems that C_D in GL2010[8] and Eurocode[9] does not consider the absence of ground effects.

4. PRESSURE COEFFICIENTS

The peak pressure coefficients are important for the wind-resistant design of components and claddings. Some accidents have occurred owing to the underestimation of peak pressure coefficients provided by current codes. Characteristics of the peak pressure coefficients are investigated by surface pressure measurements. There are two design load cases for extreme wind in IEC61400-1, that is DLC6.1 and DLC6.2. DLC6.1 is for a wind turbine with an active yaw system in which a yaw misalignment of up to $\pm 15^\circ$ should be considered. DLC6.2 assumes the loss of electrical power for control of the yaw system. In this situation, the effects of the yaw angle changing up to $\pm 180^\circ$ should be analyzed. Peak pressure coefficients for these two design load cases are discussed in this section. Distributions of the mean pressure coefficients for the component and cladding designs of nacelles are proposed and compared with the mean pressure coefficients provided by GL2010[8] and Eurocode.[9]

4.1. Definitions of pressure coefficients

The maximum $\left(\hat{C}p_{\max}\right)$ and minimum $\left(\hat{C}p_{\min}\right)$ peak pressure coefficients among all yaw angles are defined as in equations (11) and (12), respectively, to take DLC6.2 into account.

$$\hat{C}p_{\max} = Max\left\{\hat{C}p(\theta_1), \ldots, \hat{C}p(\theta_i), \ldots, \hat{C}p(\theta_n)\right\} \tag{11}$$

$$\hat{C}p_{\min} = Min\left\{\hat{C}p(\theta_1), \ldots, \hat{C}p(\theta_i), \ldots, \hat{C}p(\theta_n)\right\} \tag{12}$$

and $\hat{C}p(\theta_i)$ is peak pressure coefficient at yaw angle θ_i, expressed as follows:

$$\hat{C}p(\theta_i) = \frac{\hat{p}(\theta_i) - p_{\text{ref}}}{\frac{1}{2}\rho {V_{\text{hub}}}^2} \tag{13}$$

where $\hat{p}(\theta_i)$ is the peak pressure at a point, ρ is the air density, θ_i is the yaw angle, V_{hub} is the wind velocity at the hub height and p_{ref} is the reference pressure. The reference pressure was measured by a pitot tube placed at a distance of 1 m from the nacelle model.

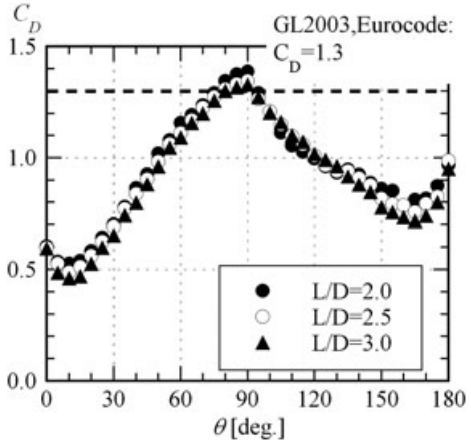

Figure 12. Comparison between C_D from the wind tunnel test and current codes.

The peak pressure coefficients for yaw angles ranging from −15° to +15° are defined as in equation (14) to take DLC6.1 into account.

$$\hat{C}p_{\max}(\pm 15^\circ) = Max\{|\hat{C}p(-15^\circ)|, \ldots, |\hat{C}p(15^\circ)|\} \tag{14}$$

4.2. Peak pressure coefficients

The distributions of maximum $(\hat{C}p_{\max})$ and minimum $(\hat{C}p_{\min})$ peak pressure coefficients for the entire range of yaw angles are shown in Figure 13. The values of the maximum peak pressure coefficients on the side and rear surfaces exceed 1.8 in the central part and decrease toward the upper and lower edges. Those on the front surface are approximately 2.0–2.2 and decrease to 1.6 in the area shielded by the hub. The maximum peak pressure coefficients on the top are nearly uniform.

As for the minimum peak pressure coefficients, the local large peak pressure coefficients are observed near each corner on all of the surfaces. The values of these local large peak pressures range from −3.0 to −5.8. The local peak pressures at each corner on the front, side and rear surface are caused by the separation flow.

The peak pressure coefficients for yaw angles ranging from −15° to +15° $(\hat{C}p_{\max}(\pm 15^\circ))$ are shown in Figure 14. The values of the peak pressure coefficients on the front surface are almost identical to the maximum peak pressure coefficients for the entire range of yaw angles. Local peak suctions appear near the front corner on the side and top surfaces, and the values range from −2.4 to −3.6. These local peak suctions are recovered toward the rear edge. The peak pressure coefficients on the rear surface decrease slightly toward each corner.

Typical variations of the maximum and minimum peak pressure coefficients with the yaw angle are shown in Figure 15. Large negative peak pressure coefficient at point 's1' near the front corner of the side surface and at point 's4' near the rear corner are observed at yaw angles of 55° and 195°, respectively. The extreme minimum peak pressure coefficients appear at the yaw angle of 215° at point 't4' on the top, and the minimum value is −5.8. This local suction is caused by conical vortices on the top at diagonal wind angles, as mentioned by Cook.[14]

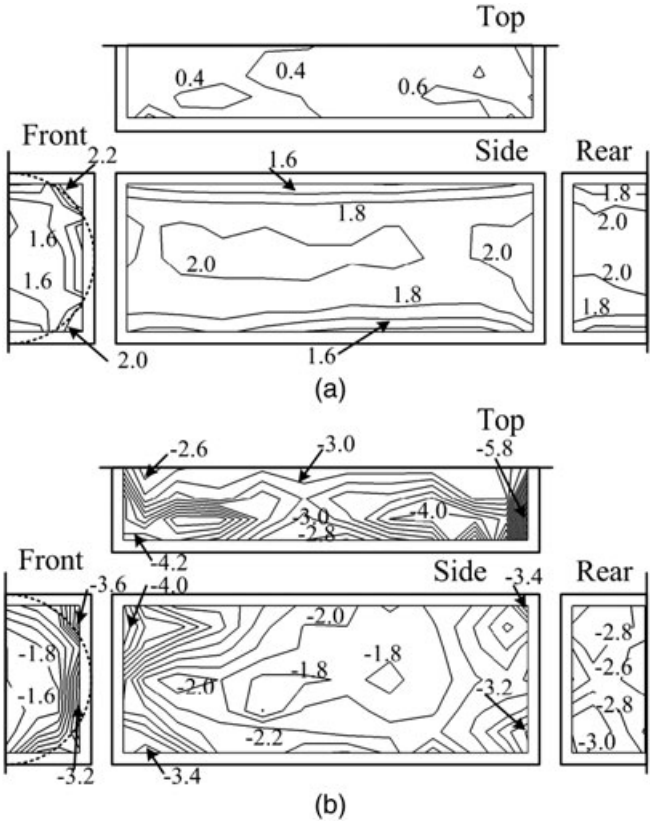

Figure 13. Maximum (a) and minimum (b) peak pressure coefficients for the entire range of yaw angles.

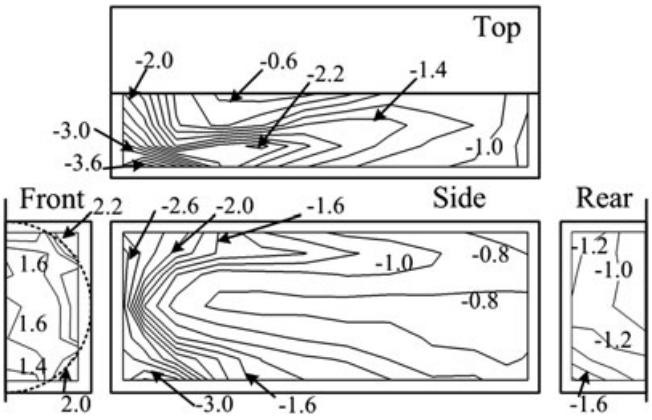

Figure 14. Maximum peak pressure coefficients for yaw angles ranging from −15° to +15°.

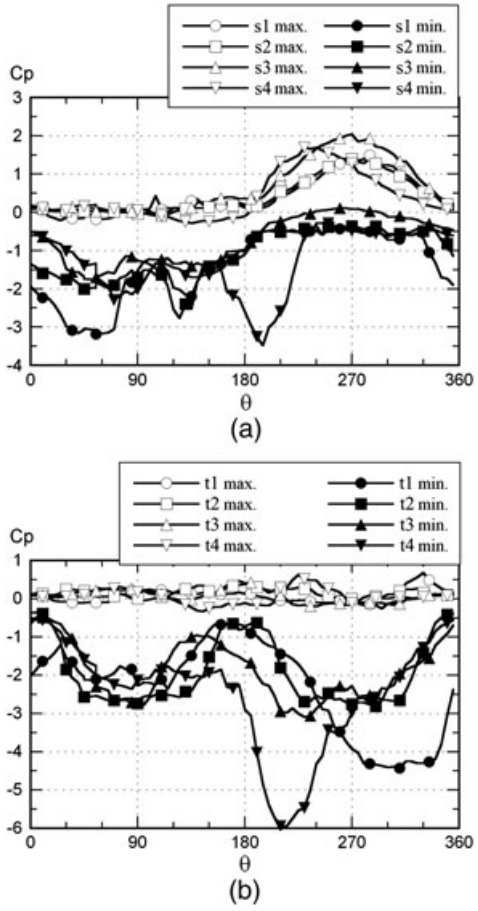

Figure 15. Variations of maximum and minimum peak pressure coefficients on (a) side surface and (b) top surface with yaw angle.

4.3. Formulas for mean pressure coefficients and comparison with current codes

Since the maximum peak pressures are primarily dominant owing to the incident turbulence, a quasisteady assumption[17] is applicable to the maximum peak pressure coefficients. In fact, distributions of the maximum peak pressure

coefficients on all of the surfaces are similar to those of the maximum mean pressure coefficients. It is difficult to directly apply a quasisteady assumption to estimate the minimum peak pressure coefficients, since the minimum peak pressure coefficients are caused by vortex shedding. In this study, the quasisteady assumption is adopted to determine the equivalent maximum and minimum peak pressure coefficients to consider the turbulence intensity in the incident flow as shown in Eurocode.[9]

The equivalent maximum ($\bar{C}pe_{\max}$) and minimum ($\bar{C}pe_{\min}$) mean pressure coefficients are defined as in equations (15) and (16), respectively.

$$\bar{C}pe_{\max} = \hat{C}p_{\max}/(1 + 7I_{\text{hub}}) \tag{15}$$

$$\bar{C}pe_{\min} = \hat{C}p_{\min}/(1 + 7I_{\text{hub}}) \tag{16}$$

I_{hub} is the turbulence intensity at the hub height, expressed as follows:

$$I_{\text{hub}} = \sigma_1/V_{\text{hub}} \tag{17}$$

where σ_1 is the standard deviation along the wind component of the incident flow.

The equivalent maximum and minimum mean pressure coefficients are proposed for DLC6.2 in IEC61400-1, as shown in Figure 16. These values are calculated using equations (15) and (16), the turbulence intensity of incident flow, and the maximum and minimum peak pressure coefficients for the entire range of yaw angles as shown in Figure 13. The turbulence intensity of the wind tunnel tests is used for determining I_{hub}. The maximum and minimum mean pressure coefficients obtained from Eurocode[9] are shown in Figure 17. The proposed equivalent

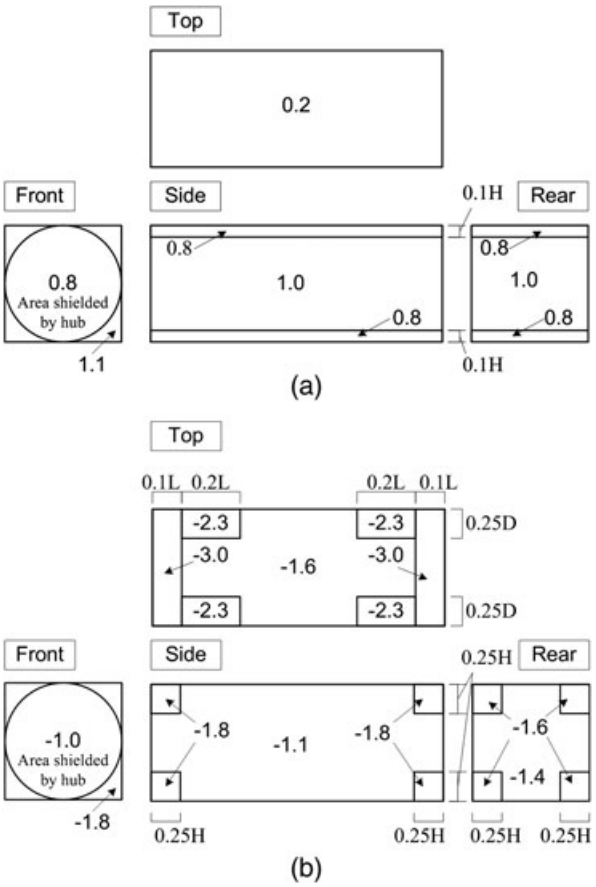

Figure 16. Equivalent maximum (a) and minimum (b) mean pressure coefficients proposed for DLC 6.2 from the wind tunnel test.

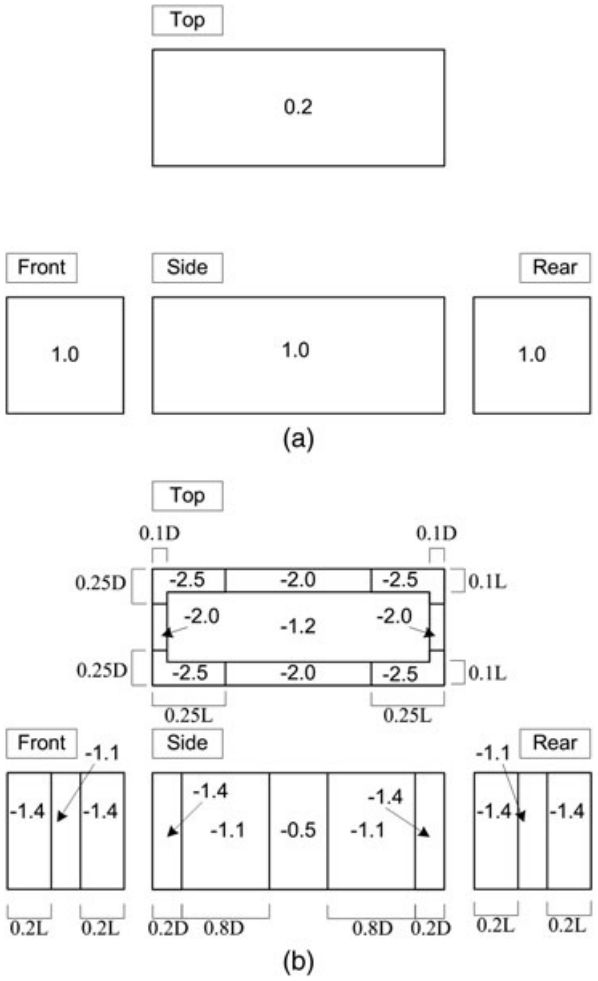

Figure 17. Maximum (a) and minimum (b) mean pressure coefficients for the entire range of yaw angles obtained from Eurocode.

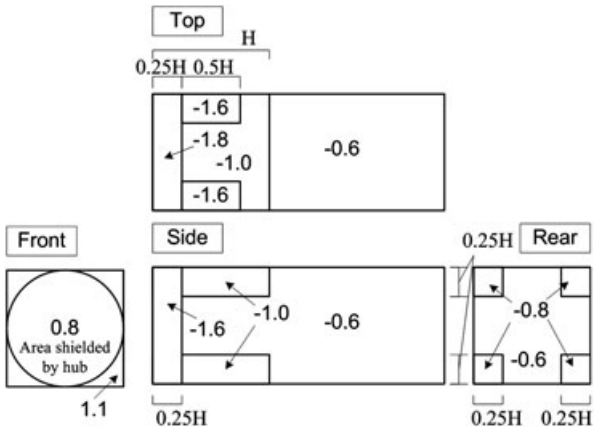

Figure 18. Mean pressure coefficients proposed for DLC6.1 from the wind tunnel test.

maximum and minimum mean pressure coefficients on the top surface are similar to those from Eurocode,[9] whereas those on the front and side surfaces are different owing to the hub and absence of effects of the ground, respectively.

The equivalent mean pressure coefficients for yaw angles ranging from -15° to $+15^\circ$ $\left(\bar{C}pe_{\max(\pm 15^\circ)}\right)$ are defined as in equation (18).

$$\bar{C}pe_{\max(\pm 15^\circ)} = \hat{C}p_{\max}(\pm 15^\circ)/(1 + 7I_{\text{hub}}) \tag{18}$$

Figure 18 shows the equivalent mean pressure coefficients proposed for DLC6.1 in IEC61400-1 based on equation (18) and the wind tunnel test results as shown in Figure 14. The mean pressure coefficients for yaw angles ranging from -45° to $+45^\circ$ provided by Eurocode[9] and the mean pressure coefficients proposed by GL2010[8] are also shown in Figures 19 and 20, respectively, for comparison. In Eurocode,[9] strong suctions located in a small region at the front of the top surface are caused by the separation flow and conical vortex. This phenomenon is typical of a rectangular prism. The mean pressure coefficients by Eurocode[9] approximate those obtained from the wind tunnel test, whereas the mean pressure coefficients near the front edge on the side and top surfaces and near each corner on the rear surface by GL2010[8] are significantly underestimated.

5. CONCLUSIONS

Wind tunnel tests are performed for measurements of the mean wind forces and peak pressures acting on wind turbine nacelles, and the results are compared with current codes. The following conclusions can be drawn from this study.

Effects of the ground and hub are observed clearly, and effects of the turbulence on the incident flow and nacelle length are negligible quite small. Formulas for C_D and C_L as functions of yaw angles are proposed. The mean wind

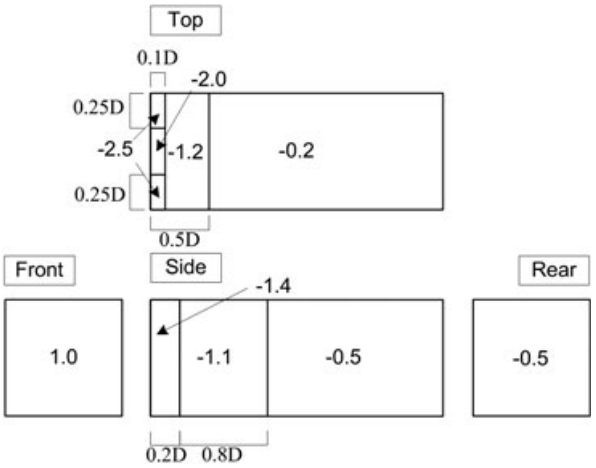

Figure 19. Mean pressure coefficients for yaw angles ranged $\pm 45^\circ$ obtained from Eurocode.

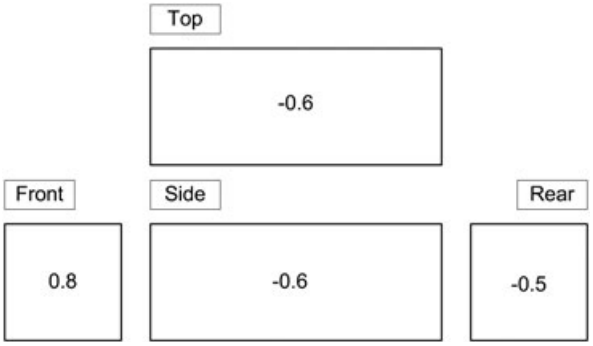

Figure 20. Mean pressure coefficients proposed by GL2010.

force coefficients of the wind turbine nacelles specified in GL2010, and Eurocode are slight underestimated in comparison with those obtained by wind tunnel tests.

The mean pressure coefficients for DLC6.2 are significantly larger than those for DLC6.1. The equivalent maximum mean pressure coefficients proposed for DLC6.1 and DLC6.2 from the pressure measurements are similar to those in Eurocode, but they are larger than those proposed in GL2010.

ACKNOWLEDGEMENTS

This study was conducted as part of the activities of the task committee on the wind-resistant design of wind turbines of the Japan Society of Civil Engineers. The proposed mean wind force and peak pressure coefficients were adopted from guidelines for the design of wind turbine support structures and foundations.[18] The authors thank Dr. K. Shimada of Shimizu Corporation for his instructive discussions.

REFERENCES

1. Garrad Hassan and Partners Limited. Generic 2 MW offshore turbine. GH Bladed Version 3.51, 2001.
2. Somers DM. Design and experimental results for the S809 airfoil. NREL/SR-6918, Golden Colorado, National Renewable Energy Lab., 1997.
3. Burton T, Sharpe D, Jenkins N, Bossanyi E. Wind Energy Handbook. Wiley, 2001.
4. DNV and RISO. Guidelines for design of wind turbines, 2003.
5. Lindenburg C. Stall coefficients—aerodynamic airfoil coefficients at large angles of attack. ECN-RX-01-004, Jan. 2001.
6. British Standards Institute. Code of basic data for the design of buildings, 1975.
7. Ishihara T, Yamaguchi A, Takahara K, Mekaru T, Matsuura S. An analysis of damaged wind turbines by typhoon Maemi in 2003. *Proc. of APCWE VI* 2005; 1413–1428.
8. Germanischer Lloyd. Guideline for the certification of wind turbines, 2010.
9. European Committee for Standardization. Eurocode 1: basis of design and actions on structures, Part 2.4. Actions on structures—wind actions, 1997.
10. IEC 61400-1. Wind turbines—Part 1: design requirement, 2005.
11. Irwin HPAH, Cooper KR, Girard R. Correction of distortion effects caused by tubing system in measurements of fluctuating pressures. *Journal of Industrial Aerodynamics* 1979; **5**: 93–107.
12. Lawson TV. Wind Effects on Building Volume 1 Design Applications. Applied Science Publisher LTD: London, 1980.
13. Aerodynamic database of low-rise buildings. [Online]. Available: http://www.wind.arch.t-kougei.ac.jp/info_center/windpressure/lowrise/mainpage.html (Accessed April 2012).
14. Cook NJ. The Designer's Guide to Wind Loading of Building Structures, Part1. Butterworths: London, 1985.
15. Noda H, Nakayama A. Free-stream turbulence effects on instantaneous pressure and forces on cylinders of rectangular cress section. *Experiments in Fluids* 2003; **34**: 332–344.
16. Nakaguchi H, Hashimoto K, Muto S. An experimental study on aerodynamic drag of rectangular cylinder. *Journal of the Japan Society of Aeronautical and Space Science* 1968; **16**: 1–15.
17. Holmes JD. Wind Loading of Structures. Taylor & Francis: London and New York, 2007.
18. Ishihara T, (ed.). Guidelines for design of wind turbine support structures and foundations, Japan Society of Civil Engineers, 2010. (in Japanese)